

# Multiple Intelligent Reflecting Surfaces Collaborative Wireless Localization System

Ziheng Zhang, Wen Chen, Qingqing Wu, Zhendong Li,  
Xusheng Zhu, Jingfeng Chen, and Nan Cheng

**Abstract**—This paper studies a multiple intelligent reflecting surfaces (IRSs) collaborative localization system where multiple semi-passive IRSs are deployed in the network to locate one or more targets based on time-of-arrival. It is assumed that each semi-passive IRS is equipped with reflective elements and sensors, which are used to establish the line-of-sight links from the base station (BS) to multiple targets and process echo signals, respectively. Based on the above model, we derive the Fisher information matrix of the echo signal with respect to the time delay. By employing the chain rule and exploiting the geometric relationship between time delay and position, the Cramér-Rao bound (CRB) for estimating the target’s Cartesian coordinate position is derived. Then, we propose a two-stage algorithmic framework to minimize CRB in single- and multi-target localization systems by joint optimizing active beamforming at BS, passive beamforming at multiple IRSs and IRS selection. For the single-target case, we derive the optimal closed-form solution for multiple IRSs coefficients design and propose a low-complexity algorithm based on alternating direction method of multipliers to obtain the optimal solution for active beaming design. For the multi-target case, alternating optimization is used to transform the original problem into two subproblems where semi-definite relaxation and successive convex approximation are applied to tackle the quadraticity and indefiniteness in the CRB expression, respectively. Finally, numerical simulation results validate the effectiveness of the proposed algorithm for multiple IRSs collaborative localization system compared to other benchmark schemes as well as the significant performance gains.

**Index Terms**—Intelligent reflecting surface, collaborative localization, time-of-arrival, Cramér-Rao bound.

## I. INTRODUCTION

The deep integration of sensing systems into future wireless networks is one of the prominent features of 6G [1]. This integration mainly includes two aspects, one of which is the rise of environment-aware applications such as self-driving [2], unmanned aerial vehicle express [3] and satellite navigation [4], and the other is reciprocity of communication and sensing, which means communication signals can be used for localization and imaging [5] while the environmental information obtained through sensing can also improve the accuracy of channel estimation and reduce pilot overhead [6]. However,

providing high-precision sensing applications in various complex electromagnetic environments faces the following key challenges. First, high-precision localization services require high-frequency and large-bandwidth sensing signals; however, their propagation suffers from stronger free-space path loss as well as atmospheric absorption and attenuation, resulting in relatively short transmission distances [1]. Then, it is difficult to establish a line-of-sight (LoS) link between the BS and the target due to various obstacles, especially in urban areas. Thus, solving the above challenges is the key to improving sensing performance in future wireless networks.

Intelligent reflecting surface (IRS) is a novel technology with the potential to address the aforementioned challenges. By forming a controllable electromagnetic field, it can reconstruct the channel and provide additional LoS links [7]. Due to its low cost, ease of deployment, and advanced integration, it has been widely used in the new generation of wireless communication. Because of the many similarities between communication and sensing systems, there have been some recent research results on how the IRS is applied to assist sensing systems [8]. Specifically, scholars have proposed three main IRS-assisted wireless sensing architectures: fully-passive IRS [9], [10], semi-passive IRS [11], [12] and IRS-self sensing systems [13]. The main difference between these three lies in the relative position of the receiving antenna and transmitter with respect to the IRS. The performance of semi-passive IRS is optimal in most cases due to its lower path loss, making it one of the mainstream designs.

In addition to the design of basic architecture, more research has focused on system design, performance analysis, and metrics selection. Detection probability is an important metric used in detection tasks in sensing. The optimal judgement threshold and closed expression for the detection probability for single target at different distances under the IRS-assisted sensing system were derived in [14]. Because the expression of detection probability regarding the signal to interference plus noise ratio (SINR) ratio contains a Q-function, it is difficult to optimize as a metric for system design. The authors utilized the monotonicity property of detection probability regarding SINR and jointly optimize active and passive beamforming in multi-target scenarios [15]. To reduce mutual interference between echo signals from different targets, three protocols, namely time division, code division, and hybrid division were also proposed in [15]. Another important task in sensing is the estimation of parameters such as position, velocity, angle, etc. The Cramér-Rao bound (CRB) is used to evaluate the minimum mean square error between an estimated value and

Z. Zhang, W. Chen, Q. Wu, X. Zhu and J. Chen are with the Department of Electronic Engineering, Shanghai Jiao Tong University, Shanghai 200240, China (e-mail: zhangziheng@sjtu.edu.cn; wenchen@sjtu.edu.cn; xushengzhu@sjtu.edu.cn; qingqingwu@sjtu.edu.cn; laowu3917@sjtu.edu.cn).

Z. Li is with the School of Information and Communication Engineering, Xi’an Jiaotong University, Xi’an 710049, China (email: lizhendong@xjtu.edu.cn).

Nan Cheng is with the School of Telecommunications Engineering, Xidian University, Xi’an 710071, China (e-mail: nancheng@xidian.edu.cn).

(Corresponding author: Wen Chen.)

the true value under unbiased estimation. In [16], the authors derived the CRB for angle and distance estimation under optimal design for fully passive IRS and proposed a low-complexity estimation algorithm based on discrete Fourier transform. Furthermore, the authors compared the system design methods and CRB for point target and extended target; and analyzed the optimal allocation of reflection elements and sensors on semi-passive IRS [17]. [18] considered the active and passive beamforming design under the integrated communication and sensing system and derived the CRB for direction-of-arrival estimation, and demonstrated the performance differences when the optimization objectives are SINR and CRB through simulation. However, the above research focuses on the derivation and optimization of CRB for of-arrival (DoA) estimation. In fact, it is difficult to uniquely determine the specific position of the target in space based solely on DoA. Research on estimation of target' specific position for IRS-assisted sensing systems needs to be conducted.

The above research on performance analysis and system optimization is based on a single IRS model. In fact, due to the convenience of the IRS, there will be a large number of IRS deployed in various places in the future [19]. In the next-generation wireless networks, the ubiquitous IRS can better serve communication and sensing applications through collaboration. First, multiple IRSs provide more observations from different angles. For multi-target sensing, multiple IRSs system can reduce the path loss of signal propagation. In [20], the authors jointly optimized the selection and beamforming among multiple IRSs to maximize energy efficiency and validated the advantages of multiple IRSs compared to single IRS and relay in simulation. The output probability of multiple IRS networks was analyzed in [21] and the asymptotic expressions for the sum-rate was also derived. The above works ignore the secondary reflection among multiple IRSs, however, secondary reflection can be used to mitigate interference between multiple users [22]. When IRSs are densely deployed in the network, there will be multiple links between the BS and the user through the reflections of different IRSs, the multi hop routing problem in multi IRS assisted communication was studied in [23]. However, very few studies have focused on multi-IRS-assisted sensing related systems. [24] provided a two-stage protocol to serve integrated sensing and communication and pure communication separately. When the system locates the target, only the sensor operates in the semi-passive IRS, which is equivalent to the traditional sensing system. In [25], the authors considered multiple IRS serving multiple targets/users simultaneously, however, this service is independent, i.e., each user or target will only receive reflective signals from one IRS. Despite the research progress, the research on multiple IRSs collaborative localization has not been carried out.

Motivated by the above considerations, we study a multiple IRSs collaborative localization system where multiple semi-passive IRSs are deployed near the base station (BS) to locate one or more targets, as shown in Fig. 1. Our objective is to minimize the CRB for estimating the position of the target in the Cartesian coordinate system by jointly optimizing the active beamforming at the BS and IRS phase shifts. The main

contributions of the paper are summarized as follows

- First, we propose a wireless localization system with multiple semi-passive IRSs collaboration, which has not been investigated in the literature. The reflective element reflects the sensing signal from the BS to the target while the sensor receives the echo signal from the target to complete the localization. To achieve orthogonality of multiplexed sensing signals, a joint design method for IRS selection and zero-forcing beamforming is proposed. Based on the above system design, we derive the Fisher information matrix (FIM) with respect to the delay of the multiplexed sensing signals passing through the target. By means of the chain rule and the geometric relationship between delay and position, we derive the CRB for the estimation of the position of the target in the Cartesian coordinate.
- Then, we propose a two-stage algorithm to minimize the derived CRB by jointly optimizing the transmitting beamforming at the BS and the reflective beamforming at the multiple IRSs. Specifically, for the single-target case, we prove the monotonicity of the CRB with respect to the received energy of the target and derive the optimal closed-form solution for reflective beamforming. Then, we propose a low-complexity algorithm based on alternating direction method of multipliers (ADMM) to obtain the optimal solution for transmitting beamforming design. For the multi-target case, we use duality to transform the max-min fairness problem into a quality-of-service (QoS) constraint problem. Due to the high coupling between IRSs coefficients and active beamforming coefficients, alternating optimization is used to transform the original problem into two subproblems. In these subproblems, semi-definite relaxation (SDR) and successive convex approximation (SCA) are applied to solve the quadraticity and indefiniteness in the CRB expression, respectively.
- Finally, numerical simulations have verified that our proposed algorithm can achieve the best system performance under various parameter settings in single- and multi-target scenarios. It is also found that a small amount of semi passive IRSs can obtain effective multi-angle observations in space. When the performance improvement approaches saturation, the performance improvement brought by more semi-passive IRS is mainly due to the increase in sensors. Next, deploying more transmitting antennas than the number of IRSs at the BS allows the algorithm to run in only one stage, which reduces the computational complexity. Moreover, the simulation results also verify the proportional relationship between CRB and the number of reflective elements, sensors, and maximum transmitting power.

The rest of this paper is as follows. In Section II, we introduce the system model of multiple IRSs collaborative localization. Then, Section III derives the closed-form estimation CRB and formulates the optimization problem. Then, in Sections IV and V, we elaborate on the two-stage optimization algorithm for the single- and multi-target localization system, respectively. Section VI reveals the performance superiority

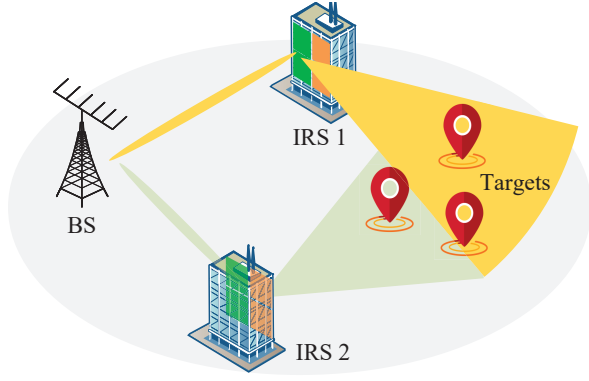


Fig. 1. Multiple IRSs collaborative localization system.

of the proposed algorithm compared to other benchmarks and some useful insights. Finally, Section VII concludes this paper.

*Notations:* Matrices, vectors and scalars are represented by bold uppercase, bold lowercase and standard lowercase letters, respectively. For a complex-valued scalar  $x$ ,  $|x|$  denotes its absolute value. For a general matrix  $\mathbf{A}$ ,  $\text{rank}(\mathbf{A})$ ,  $\mathbf{A}^H$  and  $[\mathbf{A}]_{i,j}$  denote its rank, conjugate transpose and  $(i,j)$ -th element, respectively. For a square matrix  $\mathbf{X}$ ,  $\text{rank}(\mathbf{X})$ ,  $\mathbf{X}^H$ , and  $\text{tr}(\mathbf{X})$  denote its rank, conjugate transpose, and trace.  $\mathbf{X} \succeq 0$  denotes that  $\mathbf{X}$  is a positive semidefinite matrix.  $\mathbb{C}^{M \times N}$  represents the  $M \times N$  dimensional complex matrix space.  $\mathbb{E}(\cdot)$  denotes the expectation operation.  $\sim$  represents “distributed as” and  $\mathcal{CN}(\mathbf{x}, \mathbf{R})$  represents the distribution of a circularly symmetric complex Gaussian random vector with mean vector  $\mathbf{x}$  and covariance matrix  $\mathbf{R}$ .  $\|\cdot\|_p$  represents the  $p$ -norm of a vector.  $\otimes$  represents the Kronecker product.

## II. SYSTEM MODEL

As shown in Fig. 1, the model of a multi-IRSs collaborative localization system is first introduced. We consider a IRSs-aided localization network where  $K$  semi-passive IRSs are deployed to assist in the localization system from the BS with  $N_T$  antennas to  $Q$  targets. The direct link from BS to the target is blocked because of the obstacles around the BS. Each semi-passive IRS consists of two parts:  $N$  passive reflecting elements and  $M$  active sensors. In order to distinguish the index numbers of the passive reflective elements and active sensors of the  $k$ -th semi-passive IRS, they are indexed by  $k \in \mathcal{K} = \{1, \dots, K\}$  and  $l \in \mathcal{L} = \{1, \dots, L\}$ , respectively. The location of BS,  $k$ -th IRS, and  $q$ -th target are denoted by  $\mathbf{l}_{\text{BS}} = (x_{\text{BS}}, y_{\text{BS}}, H_{\text{BS}})$ ,  $\mathbf{l}_{1,k} = (x_{1,k}, y_{1,k}, H_{1,k})$  and  $\mathbf{l}_{T,q} = (x_{T,q}, y_{T,q}, 0)$ , respectively.

### A. Channel Model

The relative direction of  $k$ -th IRS to BS is defined by  $\{\theta_{\text{B2I},k}, \varphi_{\text{B2I},k}\}$ , where  $\theta_{\text{B2I},k}$ ,  $\varphi_{\text{B2I},k}$  denote the azimuth and elevation angles from BS to  $k$ -th IRS, respectively. Here, we assume that the passive reflective elements and active sensing sensors are two uniform planar array, that is  $N = N_x \times N_z$  and  $M = M_x \times M_z$ .  $N_x$  and  $N_z$  represent the number of elements in the horizontal and vertical directions of the passive

reflective elements, respectively.  $M_x$  and  $M_z$  represent the number of elements in the horizontal and vertical directions of the active sensing sensors, respectively. The channel power gain between BS and  $k$ -th IRS can be given by  $\alpha_{\text{B2I},k}$  with  $\alpha_{\text{B2I},k} = \sqrt{\lambda^2 / 16\pi^2 d_{\text{B2I},k}^2}$ , where  $\lambda$  denotes the carrier wavelength and  $d_{\text{B2I},k}$  denotes the distance between the BS and  $k$ -th IRS. The channel from BS to  $k$ -th IRS is modeled as

$$\mathbf{H}_{\text{B2I},k} = \alpha_{\text{B2I},k} \mathbf{a}_{\text{I2B},k} \mathbf{a}_{\text{B2I},k}^H \in \mathbb{C}^{N \times N_T}, \quad (1)$$

where  $\mathbf{a}_{\text{I2B},k} = \mathbf{a}(\Phi_{\text{B2I},k}, N_x) \otimes \mathbf{a}(\Omega_{\text{B2I},k}, N_z)$  represents the receive array response vector of the passive elements on  $k$ -IRS with  $\Phi_{\text{B2I},k} = \sin(\varphi_{\text{B2I},k}) \cos(\theta_{\text{B2I},k})$ ,  $\Omega_{\text{B2I},k} = \cos(\varphi_{\text{B2I},k})$ , and  $\mathbf{a}_{\text{B2I},k} = \mathbf{a}(\Omega_{\text{B2I},k}, N_T)$  represents the transmit array response vector of the BS in the direction of the  $k$ -th IRS.  $\mathbf{a}(\tilde{\theta}, \tilde{N})$  represents the steering vector where  $\tilde{\theta}$  represents the phase difference between two adjacent elements or antennas, and  $\tilde{N}$  represents the number of antennas transmitted or received, which is defined as

$$\mathbf{a}(\tilde{\theta}, \tilde{N}) = [1, e^{j2\pi\tilde{\theta}}, \dots, e^{j2\pi(\tilde{N}-1)\tilde{\theta}}]^T \in \mathbb{C}^{\tilde{N} \times 1}. \quad (2)$$

It is assumed that  $Q$  targets are point targets in the far field of each semi-passive IRS and they are indexed by  $q \in \mathcal{Q} = \{1, \dots, Q\}$ . The angle-of-departure from passive reflecting elements to target is equal to the angle-of-arrival from passive reflective elements of  $k$ -th IRS to the active sensing sensors of  $l$ -th IRS via  $q$ -th target can be modeled as

$$\mathbf{H}_{\text{I2I},q,k,l} = \alpha_{\text{I2I},q,k,l} \mathbf{a}_{\text{T2I},q,l} \mathbf{a}_{\text{I2T},k,q}^H \in \mathbb{C}^{M \times N}, \quad (3)$$

where  $\mathbf{a}_{\text{T2I},q,l} = \mathbf{a}(\Phi_{\text{T2I},q,l}, M_x) \otimes \mathbf{a}(\Omega_{\text{T2I},q,l}, M_z)$  denotes the receive array response vector of the sensors on  $l$ -th IRS in the direction of the  $q$ -th target with  $\Phi_{\text{T2I},q,l} = \sin(\varphi_{\text{T2I},q,l}) \cos(\theta_{\text{T2I},q,l})$  and  $\Omega_{\text{T2I},q,l} = \cos(\varphi_{\text{T2I},q,l})$ ,  $\mathbf{a}_{\text{I2T},k,q} = \mathbf{a}(\Phi_{\text{I2T},k,q}, N_x) \otimes \mathbf{a}(\Omega_{\text{I2T},k,q}, N_z)$  denotes the transmit array response vector of the passive elements on  $k$ -IRS in the direction of the  $q$ -th target.  $\alpha_{\text{I2I},q,k,l} = \sqrt{\lambda^2 \kappa / 64\pi^3 d_{\text{I2T},k,q}^2 d_{\text{T2I},q,l}^2}$  denotes the path loss, where  $\kappa$  denotes the radar cross section,  $d_{\text{I2T},k,q}$  and  $d_{\text{T2I},q,l}$  denotes the distance from  $q$ -th target to  $k$ -th IRS and  $l$ -th IRS, respectively.

### B. Localization Model

Then, we introduce the model and principles of localization for semi-passive IRS system. Let  $\Theta_k = \text{diag}(\boldsymbol{\theta}_k) = \text{diag}(\alpha_{k,1} e^{j\beta_{k,1}}, \dots, \alpha_{k,N} e^{j\beta_{k,N}})$  denotes the reflection coefficient matrix of  $k$ -th IRS, where  $\alpha_{k,n}$  and  $\beta_{k,n}$  denotes the amplitude and phase reflection coefficient of the  $n$ -th element of  $k$ -th IRS, respectively. Each reflective elements of the IRS will reflect signals from BS to  $Q$  targets while each sensors of IRS will receive echo signals from  $Q$  targets. For  $l$ -th IRS, the received echo signal at its sensors can be denoted as

$$\mathbf{r}_{\text{IRS},l}(t) = \sum_{q=1}^Q \sum_{k=1}^K \mathbf{H}_{\text{I2I},q,k,l} \Theta_k \mathbf{H}_{\text{B2I},k} \cdot \mathbf{w}_k s_k(t - \tau_{\text{B2I},k} - \tau_{\text{I2T},k,q} - \tau_{\text{T2I},q,l}) + \mathbf{n}_l, \quad (4)$$

where  $\mathbf{n}_l$  represents Gaussian white noise at the sensors in  $l$ -th IRS and  $\mathbf{n}_l \sim \mathcal{CN}(0, \sigma_l^2 \mathbf{I}_M)$ ;  $\tau_{\text{B2I},k}$  represents the time-of-arrival (TOA) from BS to  $k$ -th IRS. Because the location of the BS and IRS is fixed,  $\tau_{\text{B2I},k}$  is known and useless for localization.  $\tau_{\text{T2I},q,l}$  represent the TOA from  $q$ -th target to  $l$ -th IRS.  $\tau_{\text{I2T},k,q}$  and  $\tau_{\text{T2I},q,l}$  are unknown and key parameters in the localization system. Based on the elliptical localization method,  $\tau_{\text{I2T},k,q}$  and  $\tau_{\text{T2I},q,l}$  are viewed as a whole, so we define  $\tau_{q,k,l} \triangleq \tau_{\text{I2T},k,q} + \tau_{\text{T2I},q,l}$ . The relationship between  $\tau_{q,k,l}$  and location of the  $q$ -th target can be expressed as

$$c\tau_{q,k,l} = \|\mathbf{I}_{l,k} - \mathbf{I}_{T,q}\|_2 + \|\mathbf{I}_{l,l} - \mathbf{I}_{T,q}\|_2. \quad (5)$$

### III. CRB PERFORMANCE FOR TARGETS' ESTIMATION AND PROBLEM FORMULATION

#### A. Cramér-Rao Bound

CRB provides a lower bound of variance of any unbiased estimator, given the location vector to be estimated of  $Q$  targets  $\mathbf{u} = [\mathbf{u}_1, \dots, \mathbf{u}_Q]^T = [x_{T,1}, y_{T,1}, \dots, x_{T,Q}, y_{T,Q}]^T \in \mathbb{R}^{2Q}$ . For each element in  $\mathbf{u}$ , the variance of the unbiased estimator  $\hat{\mathbf{u}}_i$  satisfies

$$\text{var}(\hat{\mathbf{u}}_i) \geq [\mathbf{C}_{CRB}(\mathbf{u})]_{i,i} = [\mathbf{F}^{-1}(\mathbf{u})]_{i,i}, i = 1, 2, \dots, 2Q, \quad (6)$$

where  $\mathbf{C}_{CRB}(\mathbf{u})$  and  $\mathbf{F}^{-1}(\mathbf{u})$  denote the CRB matrix and FIM of  $\mathbf{u}$  to be estimated, respectively. However, it's difficult to calculate the FIM with respect to  $\mathbf{u}$  directly. Accordingly, we choose to calculate the FIM with respect to  $\boldsymbol{\tau} \in \mathbb{R}^{Q \cdot K^2}$  first, where  $\boldsymbol{\tau} = [\tau_{1,1,1}, \dots, \tau_{1,K,K}, \dots, \tau_{Q,K,K}]$  and apply the chain rule to drive the  $\mathbf{F}(\mathbf{u})$ . Specifically,  $\mathbf{F}(\mathbf{u})$  can be represented as

$$\mathbf{F}(\mathbf{u}) = \frac{\partial \boldsymbol{\tau}}{\partial \mathbf{u}} \mathbf{F}(\boldsymbol{\tau}) \left( \frac{\partial \boldsymbol{\tau}}{\partial \mathbf{u}} \right)^T \in \mathbb{R}^{2Q \times 2Q}. \quad (7)$$

Applying the theory of matrix partitioning,  $\mathbf{F}(\boldsymbol{\tau})$  has the following form

$$\mathbf{F}(\boldsymbol{\tau}) = \begin{bmatrix} \mathbf{F}_{1,1} & \mathbf{F}_{1,2} & \cdots & \mathbf{F}_{1,Q} \\ \mathbf{F}_{1,2}^H & \mathbf{F}_{2,2} & \cdots & \mathbf{F}_{2,Q} \\ \vdots & \vdots & \ddots & \vdots \\ \mathbf{F}_{1,G}^H & \mathbf{F}_{1,G-1}^H & \cdots & \mathbf{F}_{Q,Q} \end{bmatrix} \in \mathbb{R}^{GK^2 \times GK^2}, \quad (8)$$

where the  $((k_1 - 1)K + l_1, (k_2 - 1)K + l_2)$ -th element of submatrix  $\mathbf{F}_{q_1, q_2}$  is given by

$$[\mathbf{F}_{q_1, q_2}]_{(k_1-1)K+l_1, (k_2-1)K+l_2} = \mathbb{E}_{\mathbf{r}_{\text{IRS}}|\boldsymbol{\tau}} \left[ \frac{\partial^2 \log p(\mathbf{r}_{\text{IRS}}|\boldsymbol{\tau})}{\partial \tau_{q_1, k_1, l_1} \partial \tau_{q_2, k_2, l_2}} \right], \quad (9)$$

$(k_1, k_2, l_1, l_2 \in \mathcal{K}, q_1, q_2 \in \mathcal{Q})$

where  $\mathbf{r}_{\text{IRS}} = [\mathbf{r}_{\text{IRS},1}, \mathbf{r}_{\text{IRS},2}, \dots, \mathbf{r}_{\text{IRS},K}]$  represents the echo signal observations collected by active sensors of  $K$  IRSs,  $p(\mathbf{r}_{\text{IRS}}|\boldsymbol{\tau})$  is the joint probability density function of  $\mathbf{r}_{\text{IRS}}$  conditioned on  $\boldsymbol{\tau}$  and can be given by [26]

$$p(\mathbf{r}_{\text{IRS}}|\boldsymbol{\tau}) = \exp \left( -\frac{1}{\sigma_l^2} \sum_{l=1}^K \int_T |\mathbf{r}_{\text{IRS},l}(t) - \overline{\mathbf{r}_{\text{IRS},l}}(t)|^2 dt \right), \quad (10)$$

where  $\overline{\mathbf{r}_{\text{IRS},l}}(t)$  denotes the deterministic component of the received echo signal.

It is assumed that  $G$  targets all are isolated. Specifically, arbitrarily different two targets  $q_1$  and  $q_2$  are said to be separable over the  $k$ - $l$  path, which means the signal reflected from elements of  $k$ -th IRS and received at sensors of  $l$ -th IRS. If the radar effective pulse width is  $\tau_r$ , the following inequalities hold [27]

$$|\tau_{q_1, k_1, l_1} - \tau_{q_2, k_2, l_2}| > \tau_r, \forall q_1 \neq q_2, k_1, k_2, l_1, l_2. \quad (11)$$

Based on the above assumptions, echo signals from different targets are separable in the time domain and do not interfere with each other. Therefore, based on (9) and (10),  $[\mathbf{F}_{q_1, q_2}]_{(k_1-1)K+l_1, (k_2-1)K+l_2}$  is denoted as (12) and the detail is shown in Appendix A, where  $\mathbf{H}_{q, k, l} = \mathbf{H}_{\text{I2I}, q, k, l} \boldsymbol{\Theta}_k \mathbf{H}_{\text{B2I}, k}$  and  $\dot{s}_k(t - \tau_{q, k, l}) = \frac{\partial s_k(t - \tau_{q, k, l})}{\partial \tau_{q, k, l}}$ . Although the echo signals from different targets do not interfere, the reflected signals from passive units of different IRSs reflected by the same target can interfere with each other when they are received at the sensor. To ensure that sensors can distinguish different delay signals of the same target, reflected signals from different IRS must be orthogonal, i.e.

$$\mathbf{H}_{\text{I2I}, k_1, l} \boldsymbol{\Theta}_{k_1} \mathbf{H}_{\text{B2I}, k_1} \mathbf{w}_{k_2} = \mathbf{0}, k_1 \neq k_2. \quad (13)$$

To meet above constraints, we can design the beam assignment of the BS to achieve orthogonality of the reflected signals or zeros the amplitudes of IRSs, i.e.,

$$\mathbf{a}^H(\Omega_{\text{B2I}, k_1}, N_T) \mathbf{w}_{k_2} = 0, k_1 \neq k_2 \text{ or } \boldsymbol{\Theta}_{k_1} = \mathbf{0}_{K \times K}. \quad (14)$$

In the subsequent system design, we propose a two-stage algorithm to minimize the CRB by using above two methods simultaneously. Based (14),  $[\mathbf{F}_{q_1, q_2}]_{(k_1-1)K+l_1, (k_2-1)K+l_2}$  is denoted as

$$[\mathbf{F}_{q_1, q_2}]_{(k_1-1)K+l_1, (k_2-1)K+l_2} = \begin{cases} \frac{\eta}{\sigma_l^2} \|\mathbf{H}_{q_1, k_1, l} \mathbf{w}_{k_1}\|_2^2, & q_1 = q_2, k_1 = k_2 \text{ and } l_1 = l_2, \\ 0, & \text{others,} \end{cases} \quad (15)$$

where  $\eta = \int_T \dot{s}_{k_1}(t - \tau_{q_1, k_1, l_1}) \dot{s}_{k_1}^*(t - \tau_{q_1, k_1, l_1}) dt$ . Then, we calculate the relationship between time delay and position  $\frac{\partial \boldsymbol{\tau}}{\partial \mathbf{u}}$ , which can be given by matrix partitioning as follows

$$\frac{\partial \boldsymbol{\tau}}{\partial \mathbf{u}} = \begin{bmatrix} \frac{\partial \boldsymbol{\tau}}{\partial \mathbf{u}_1} & \cdots & \mathbf{0}_{2 \times K^2} \\ \vdots & \ddots & \vdots \\ \mathbf{0}_{2 \times K^2} & \cdots & \frac{\partial \boldsymbol{\tau}}{\partial \mathbf{u}_Q} \end{bmatrix} \in \mathbb{R}^{2Q \times K^2}, \quad (16)$$

where  $\frac{\partial \boldsymbol{\tau}}{\partial \mathbf{u}_q}$  can be given by

$$\frac{\partial \boldsymbol{\tau}}{\partial \mathbf{u}_q} = \begin{bmatrix} \frac{\partial \tau_{1,1,1}}{\partial x_{T,q}} & \cdots & \frac{\partial \tau_{1,K,K}}{\partial x_{T,q}} \\ \frac{\partial \tau_{1,1,1}}{\partial y_{T,q}} & \cdots & \frac{\partial \tau_{1,K,K}}{\partial y_{T,q}} \end{bmatrix} \in \mathbb{R}^{2 \times K^2}. \quad (17)$$

Based on (5), The derivative of the time delay with respect to the coordinates  $\frac{\partial \tau_{q, k, l}}{\partial x_{T,q}}$  and  $\frac{\partial \tau_{q, k, l}}{\partial y_{T,q}}$  can be denoted as (18) and (19), respectively. In order to more clearly represent the geometric relationship between the target and multiple IRSs, we explain the meaning of the angles mentioned in Fig. 2.

$$[\mathbf{F}_{q_1, q_2}]_{(k_1-1)K+l_1, (k_2-1)K+l_2} = \begin{cases} 0, l_1 \neq l_2 \text{ or } q_1 \neq q_2, \\ \frac{1}{\sigma_l^2} \text{Re} \int_T \left[ \mathbf{H}_{q_1, l_1, k} \mathbf{H}_{q_2, l_2, k}^H \sum_{k=1}^K \mathbf{w}_k^H \dot{s}_k^H (t - \tau_{q_1, l_1, k}) \sum_{k=1}^K \mathbf{w}_k \dot{s}_k (t - \tau_{q_2, l_2, k}) \right] dt, \text{ others,} \end{cases} \quad (12)$$

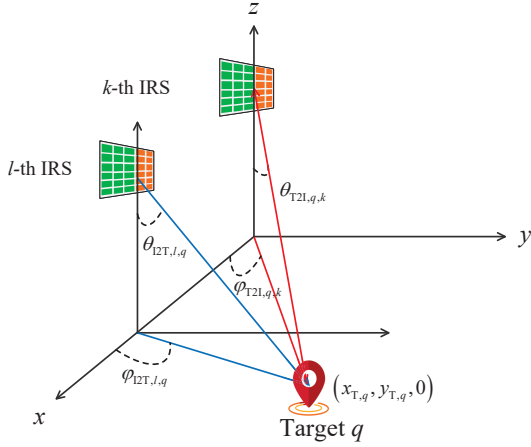


Fig. 2. Relative angle between multiple IRSs and target.

Recalling (7), (8), (16) and (17), the FIM for all  $Q$  targets can be represented as

$$\mathbf{F}(\mathbf{u}) = \begin{bmatrix} \frac{\partial \tau}{\partial \mathbf{u}_1} \mathbf{F}_{1,1} \frac{\partial \tau^T}{\partial \mathbf{u}_1} & \cdots & \mathbf{0}_{2 \times 2} \\ \vdots & \ddots & \vdots \\ \mathbf{0}_{2 \times 2} & \cdots & \frac{\partial \tau}{\partial \mathbf{u}_Q} \mathbf{F}_{Q,Q} \frac{\partial \tau^T}{\partial \mathbf{u}_Q} \end{bmatrix} \triangleq \begin{bmatrix} \mathbf{G}_1 & \cdots & \mathbf{0}_{2 \times 2} \\ \vdots & \ddots & \vdots \\ \mathbf{0}_{2 \times 2} & \cdots & \mathbf{G}_Q \end{bmatrix}. \quad (20)$$

For the  $q$ -th target, the CRB of its location  $(x_{T,q}, y_{T,q})$  is given by (21), where  $c_0$  is a constant.

### B. Problem Formulation

Let  $\boldsymbol{\theta} = [\boldsymbol{\theta}_1, \dots, \boldsymbol{\theta}_K] \in \mathbb{C}^{N \times K}$  and  $\mathbf{W} = [\mathbf{w}_1, \dots, \mathbf{w}_K] \in \mathbb{C}^{N_T \times K}$ . In this paper, we aim to minimize the maximum CRB of estimation of  $Q$  targets' location by jointly optimizing the transmit beamforming  $\mathbf{W}$  at the BS and reflect beamforming  $\boldsymbol{\theta}$  at the IRSs, subject to maximum transmit power constraints. The corresponding optimization problem is formulated as

$$(P1): \min_{\boldsymbol{\theta}, \mathbf{W}} \max_q \text{CRB}(x_{T,q}, y_{T,q}) \quad (22a)$$

$$\text{s.t. } \mathbf{H}_{q, k_1, l} \mathbf{w}_{k_2} = \mathbf{0}, k_1 \neq k_2, \forall k_1, k_2, q, \quad (22b)$$

$$\text{tr}(\mathbf{W}\mathbf{W}^H) = P_{\max}, \quad (22c)$$

$$0 \leq \alpha_{k,n} \leq 1, \forall k, n, \quad (22d)$$

$$0 \leq \beta_{k,n} < 2\pi, \forall k, n. \quad (22e)$$

where  $P_{\max}$  denotes the maximum transmitting power of the BS. Note that the objective function is non-convex due to the

coupling  $\boldsymbol{\theta}$  and  $\mathbf{W}$  in targets' CRB expressions. In addition, the constraints in (22b) are bilinear equation constraints and can not be tackled by existing methods. In this paper, we propose a new two-stage algorithm to solve (P1) and show that by applying reasonable reformulations to the CRB expression in (P1), the problem can be efficiently solved with high-quality solutions.

## IV. SINGLE-TARGET SYSTEM

In this section, we consider the single-target scenario, i.e.,  $Q = 1$ , where only one target needs to be localized in the time-frequency domain. In this case, echo signals for localization of different targets are distinguished in the time or frequency domain. Therefore, (P1) is simplified to

$$(P2): \min_{\boldsymbol{\theta}, \mathbf{W}} \text{CRB}(x_{T,1}, y_{T,1}) \quad (23a)$$

$$\text{s.t. } \mathbf{H}_{1, k_1, l} \mathbf{w}_{k_2} = \mathbf{0}, k_1 \neq k_2, \forall k_1, k_2, \quad (23b)$$

$$\text{tr}(\mathbf{W}\mathbf{W}^H) = P_{\max}, \quad (23c)$$

$$0 \leq \alpha_{k,n} \leq 1, \forall k, n, \quad (23d)$$

$$0 \leq \beta_{k,n} < 2\pi, \forall k, n. \quad (23e)$$

Although much simplified, (P2) is still a non-convex optimization problem because of the (23b) and coupled  $\boldsymbol{\theta}$  and  $\mathbf{W}$ . In this section, we propose a two-stage ADMM-based algorithm to solve (P2). Specifically, in the first stage, we activate all IRS reflective elements and achieve orthogonality required in (23b) only by active beamforming at BS; in the second stage, we achieve orthogonality by joint active and passive beamforming.

### A. Reflective Beamforming Design

First, in the first stage, we do not consider the case  $\boldsymbol{\Theta}_k = \mathbf{0}_{K \times K}$  and assume  $\mathbf{a}^H(\Omega_{B2l, k_1}, N_T) \mathbf{w}_{k_2} = 0, k_1 \neq k_2$ . Specifically, (P2) can be reduce to

$$(P2.1): \min_{\boldsymbol{\theta}, \mathbf{W}} \text{CRB}(x_{T,1}, y_{T,1}) \quad (24a)$$

$$\text{s.t. } \mathbf{a}^H(\Omega_{B2l, k_1}, N_T) \mathbf{w}_{k_2} = 0, k_1 \neq k_2, \quad (24b)$$

$$(23c), (23d), (23e).$$

Prior to solving (P2.1), we first analyze the relationship between CRB and beam energy.

*Proposition 1:*  $\text{CRB}(x_{T,1}, y_{T,1})$  monotonically non-increasing with the increase of  $\|\mathbf{H}_{1, k, l} \mathbf{w}_k\|_2^2$ .

*Proof:* Let

$$\mathbf{G}_{1, k, l} = \begin{bmatrix} a_{1, k, l}^2 & a_{1, k, l} b_{1, k, l} \\ a_{1, k, l} b_{1, k, l} & b_{1, k, l}^2 \end{bmatrix} \in \mathbb{R}^{2 \times 2}. \quad (25)$$

$\mathbf{G}_1$  can be represented as  $\mathbf{G}_1 = \sum_{k=1}^K \sum_{l=1}^K |\mathbf{H}_{1, k, l} \mathbf{w}_k|_2^2 \mathbf{G}_{1, k, l}$ . It's obvious that  $\mathbf{G}_{1, k, l}$  is a semi-positive definite matrix and

$$\frac{\partial \tau_{q,k,l}}{\partial x_{T,q}} = \frac{-1}{c} [(\sin \varphi_{12T,k,q} \cos \theta_{12T,k,q}) + (\sin \varphi_{T21,q,l} \cos \theta_{T21,q,l})] \triangleq \frac{-1}{c} a_{q,k,l}, \quad (18)$$

$$\frac{\partial \tau_{q,k,l}}{\partial y_{T,q}} = \frac{-1}{c} [(\sin \varphi_{12T,k,q} \sin \theta_{12T,k,q}) + (\sin \varphi_{T21,q,l} \sin \theta_{T21,q,l})] \triangleq \frac{-1}{c} b_{q,k,l}. \quad (19)$$

$$\begin{aligned} \text{CRB}(x_{T,q}, y_{T,q}) &= \text{tr}(\mathbf{G}_q^{-1}) = c_0 \text{tr} \left( \begin{bmatrix} \sum_{k=1}^K \sum_{l=1}^K a_{q,k,l}^2 |\mathbf{H}_{q,k,l} \mathbf{w}_k|_2^2 & \sum_{k=1}^K \sum_{l=1}^K a_{q,k,l} b_{q,k,l} |\mathbf{H}_{q,k,l} \mathbf{w}_k|_2^2 \\ \sum_{k=1}^K \sum_{l=1}^K a_{q,k,l} b_{q,k,l} |\mathbf{H}_{q,k,l} \mathbf{w}_k|_2^2 & \sum_{k=1}^K \sum_{l=1}^K b_{q,k,l}^2 |\mathbf{H}_{q,k,l} \mathbf{w}_k|_2^2 \end{bmatrix}^{-1} \right) \\ &= c_0 \frac{\sum_{k=1}^K \sum_{l=1}^K a_{q,k,l}^2 |\mathbf{H}_{q,k,l} \mathbf{w}_k|_2^2 + \sum_{k=1}^K \sum_{l=1}^K b_{q,k,l}^2 |\mathbf{H}_{q,k,l} \mathbf{w}_k|_2^2}{\left( \sum_{k=1}^K \sum_{l=1}^K a_{q,k,l}^2 |\mathbf{H}_{q,k,l} \mathbf{w}_k|_2^2 \right) \left( \sum_{k=1}^K \sum_{l=1}^K b_{q,k,l}^2 |\mathbf{H}_{q,k,l} \mathbf{w}_k|_2^2 \right) - \left( \sum_{l=1}^K \sum_{k=1}^K a_{q,k,l} b_{q,k,l} |\mathbf{H}_{q,k,l} \mathbf{w}_k|_2^2 \right)^2}. \end{aligned} \quad (21)$$

$|\mathbf{H}_{1,k,l} \mathbf{w}_k|_2^2 \geq 0$ . Therefore,  $\mathbf{G}_1$  is a semi-positive definite matrix with two eigenvalues are  $\lambda_1$  and  $\lambda_2$ ,  $\lambda_1 \geq \lambda_2 \geq 0, \lambda_1 \lambda_2 \neq 0$ .

Without loss of generality, we assume that the increment of  $\|\mathbf{H}_{1,k,l} \mathbf{w}_k\|_2^2$  is  $\Delta |\mathbf{H}_{1,k,l} \mathbf{w}_k|_2^2$  and the corresponding matrix is  $\mathbf{G}'_1$  after the increase, which can be represented as

$$\mathbf{G}'_1 = \mathbf{G}_1 + \Delta |\mathbf{H}_{1,k,l} \mathbf{w}_k|_2^2 \mathbf{G}_{1,k,l}. \quad (26)$$

Similarly,  $\mathbf{G}'_1$  is a semi-positive definite matrix with two eigenvalues are  $\lambda'_1$  and  $\lambda'_2$ ,  $\lambda'_1 \geq \lambda'_2 \geq 0, \lambda'_1 \lambda'_2 \neq 0$ . According to Weyl inequality, we have  $\lambda'_1 \geq \lambda_1, \lambda'_2 \geq \lambda_2$ . Therefore,

$$\text{tr} \left( \left( \mathbf{G}'_1 \right)^{-1} \right) = \frac{1}{\lambda'_1} + \frac{1}{\lambda'_2} \leq \frac{1}{\lambda_1} + \frac{1}{\lambda_2} = \text{tr}(\mathbf{G}_1^{-1}). \quad (27)$$

The proof is completed.  $\blacksquare$

Based on Proposition 1, the design of  $\Theta_k$  is supposed to maximize  $\|\mathbf{H}_{1,k,l} \mathbf{w}_k\|_2^2$ , which can be represented as  $\alpha_{121,1,k,l}^2 M \|\mathbf{a}_R^H(\Phi_{12T,k,1}, \Omega_{12T,k,1}) \text{diag}(\mathbf{H}_{B21,k} \mathbf{w}_k) \boldsymbol{\theta}_k\|_2^2$ . Accordingly, the optimal design of  $\Theta_k$  is given by

$$\boldsymbol{\theta}_k = \frac{(\mathbf{a}_R^H(\Phi_{12T,k,1}, \Omega_{12T,k,1}) \text{diag}(\mathbf{H}_{B21,k} \mathbf{w}_k))^*}{|\mathbf{a}_R^H(\Phi_{12T,k,1}, \Omega_{12T,k,1}) \text{diag}(\mathbf{H}_{B21,k} \mathbf{w}_k)|}. \quad (28)$$

### B. Transmitting Beamforming Design

In the first stage, the transmitting beamforming design is supposed to satisfy  $\mathbf{a}^H(\Omega_{B21,k_1}, N_T) \mathbf{w}_{k_2} = 0, k_1 \neq k_2$ . Therefore, the feasible design is given by

$$\mathbf{W} = \mathbf{A}_{B21}^H (\mathbf{A}_{B21} \mathbf{A}_{B21}^H)^{-1} \mathbf{E}, \quad (29)$$

where  $\mathbf{A}_{B21} = [\mathbf{a}_{B21,1}^H, \dots, \mathbf{a}_{B21,K}^H] \in \mathbb{C}^{K \times N_T}$  and  $\mathbf{E} = \text{diag}(\mathbf{e}) = \text{diag}([e_1, \dots, e_K]) \in \mathbb{R}^{K \times K}$  denotes the transmitting power allocation over different beams. According to the transmitting power constraint (22c), we have

Let  $\alpha_{k,l} = \alpha_{121,1,k,l}^2 \alpha_{B21,k}^2 M N^2$ ,  $a_k = \sum_{l=1}^K a_{1,k,l}^2 \alpha_{k,l}$ ,  $b_k = \sum_{l=1}^K b_{1,k,l}^2 \alpha_{k,l}$  and  $c_k = \sum_{l=1}^K a_{1,k,l} b_{1,k,l} \alpha_{k,l}$ . Based on (28), (29) and above definition, (P2.1) is equivalent to

$$\text{(P2.2)}: \min_{\mathbf{e}} \frac{\sum_{k=1}^K e_k^2 a_k + \sum_{k=1}^K e_k^2 b_k}{\left( \sum_{k=1}^K e_k^2 a_k \right) \left( \sum_{k=1}^K e_k^2 b_k \right) - \left( \sum_{k=1}^K e_k^2 c_k \right)^2} \quad (30a)$$

$$\text{s.t.} \quad \sum_{k=1}^K e_k^2 \left[ (\mathbf{A}_{B21} \mathbf{A}_{B21}^H)^{-1} \right]_{k,k} = P_{\max}, \quad (30b)$$

which is also difficult to solve because it is a fractional programming and the denominator is non-convex. For the convenience of representation, we use vector form to equivalently represent the problem as

$$\text{(P2.3)}: \min_{\mathbf{p}} \frac{(\mathbf{a}^T + \mathbf{b}^T) \mathbf{p}}{\mathbf{p}^T (\mathbf{a} \mathbf{b}^T - \mathbf{c} \mathbf{c}^T) \mathbf{p}} \quad (31a)$$

$$\text{s.t.} \quad \mathbf{h}^T \mathbf{p} = P_{\max}, \quad (31b)$$

$$p_k \geq 0, \forall k, \quad (31c)$$

where  $\mathbf{p} = [e_1^2, \dots, e_K^2]^T$ ,  $p_k$  denotes the  $k$ -th element in  $\mathbf{p}$ ,  $\mathbf{a} = [a_1, \dots, a_K]^T$ ,  $\mathbf{b} = [b_1, \dots, b_K]^T$ ,  $\mathbf{c} = [c_1, \dots, c_K]^T$ ,  $\mathbf{h} = \left[ \left[ (\mathbf{A}_{B21} \mathbf{A}_{B21}^H)^{-1} \right]_{1,1}, \dots, \left[ (\mathbf{A}_{B21} \mathbf{A}_{B21}^H)^{-1} \right]_{K,K} \right]^T$ .

Since  $\mathbf{a} \mathbf{b}^T - \mathbf{c} \mathbf{c}^T$  is an indefinite matrix, we introduce additional auxiliary  $\mathbf{z}$  to deal with non-convexity in the denominator and penalty term  $\frac{\rho}{2} \|\mathbf{p} - \mathbf{z}\|_2^2$  to ensure equivalence with the original expression. Specifically,  $\mathbf{p}^T (\mathbf{a} \mathbf{b}^T - \mathbf{c} \mathbf{c}^T) \mathbf{p}$  can be represented as

$$f_d(\mathbf{p}, \mathbf{z}) \triangleq \mathbf{p}^T (\mathbf{A} - \beta) \mathbf{p} + \beta \mathbf{z}^T \mathbf{z} - \frac{\rho}{2} \|\mathbf{p} - \mathbf{z}\|_2^2, \quad (32)$$

where  $\mathbf{A} = \frac{1}{2} (\mathbf{a} \mathbf{b}^T + \mathbf{b} \mathbf{a}^T)$  and  $\beta$  is the maximum eigenvalue of  $\mathbf{A}$ ,  $\rho/2$  is a penalty factor and should be greater than  $\beta$ . The above restriction on the  $\beta$  and  $\rho$  ensures that (32) is a

concave function with respect to  $\mathbf{p}$  and  $\mathbf{z}$ . Then, by utilizing the Dinkelbach's transform, the original fractional planning can be transformed into the following form

$$(P2.4): \min_{\mathbf{p}, \mathbf{z}} \alpha (\mathbf{a}^T + \mathbf{b}^T) \mathbf{p} - f_d(\mathbf{p}, \mathbf{z}) \quad (33a)$$

$$\text{s.t. } \mathbf{h}^T \mathbf{z} = P_{\max}, \quad (33b)$$

$$z_k \geq 0, \forall k, \quad (33c)$$

$$\mathbf{p} = \mathbf{z}, \quad (33d)$$

where  $z_k$  is the  $k$ -th element in  $\mathbf{z}$  and  $\alpha$  is a new auxiliary variable, which is updated by

$$\alpha[t+1] = \frac{f_d(\mathbf{p}[t], \mathbf{z}[t])}{(\mathbf{a}^T + \mathbf{b}^T) \mathbf{p}[t]}, \quad (34)$$

where  $t$  is the iteration index. To solve (P2.4), we employ ADMM method to handle the equation constraints (33d). The augmented Lagrangian function of (P2.4) can be expressed as

$$L(\mathbf{p}, \mathbf{z}, \boldsymbol{\lambda}) = \alpha (\mathbf{a}^T + \mathbf{b}^T) \mathbf{p} - f_d(\mathbf{p}, \mathbf{z}) + \boldsymbol{\lambda}^T (\mathbf{p} - \mathbf{z}), \quad (35)$$

where  $\boldsymbol{\lambda}$  is Lagrange multiplier. The variables can be divided into three blocks and updated sequentially by solving the corresponding subproblems. Specifically, the subproblems and their solutions are elaborated as follows.

#### 1) Subproblem with respect to $\mathbf{p}$

For optimizing  $\mathbf{p}$ , we consider the following subproblem

$$\min_{\mathbf{p}} \alpha (\mathbf{a}^T + \mathbf{b}^T) \mathbf{p} - f_d(\mathbf{p}, \mathbf{z}) + \boldsymbol{\lambda}^T (\mathbf{p} - \mathbf{z}), \quad (36)$$

which is a standard convex problem and can be solved by the first order optimality condition, i.e.,

$$\mathbf{p}[s+1] = \left( \mathbf{a}\mathbf{b}^T - \mathbf{c}\mathbf{c}^T - \beta\mathbf{I} - \frac{\rho}{2}\mathbf{I} \right)^{-1} \cdot \left( \frac{\alpha(\mathbf{a} + \mathbf{b}) + \boldsymbol{\lambda}[s] - \rho\mathbf{z}[s]}{2} \right) \quad (37)$$

#### 2) Subproblem with respect to $\mathbf{z}$

For optimizing  $\mathbf{z}$  with fixing the other variables, the corresponding subproblem is reduced to

$$(P2.5): \min_{\mathbf{z}} \frac{\rho}{2} \|\mathbf{p} - \mathbf{z}\|_2^2 - \beta \mathbf{z}^T \mathbf{z} + \boldsymbol{\lambda}^T (\mathbf{p} - \mathbf{z}) \quad (38a)$$

$$\text{s.t. } (33b), (33c)$$

The Lagrangian function of this subproblem can be formulated as

$$L(\mathbf{z}, \mu_0, \boldsymbol{\mu}) = \frac{\rho}{2} \|\mathbf{p} - \mathbf{z}\|_2^2 - \beta \mathbf{z}^T \mathbf{z} + \boldsymbol{\lambda}^T (\mathbf{p} - \mathbf{z}) + \mu_0 (\mathbf{h}^T \mathbf{z} - P_{\max}) + \boldsymbol{\mu}^T \mathbf{z}, \quad (39)$$

where  $\mu_0$  and  $\boldsymbol{\mu} = [\mu_1, \dots, \mu_K]^T$  are Lagrange multipliers. (P2.5) is a convex problem and can be solved according to Karush-Kuhn-Tucker (KKT) conditions. The optimal solution to (P2.4) is given by

$$z_i = \begin{cases} \frac{(\lambda_i + \rho p_i - \mu_0 h_i)}{2(\frac{\rho}{2} - \beta)}, \mu_0 < \frac{\lambda_i + \rho p_i}{h_i}, \\ 0, \mu_0 \geq \frac{\lambda_i + \rho p_i}{h_i}, \end{cases} \quad (40)$$

---

### Algorithm 1 Proposed ADMM-based Algorithm.

---

- 1: **Input:** Initialize  $\alpha, \mathbf{p}, \mathbf{z}, \boldsymbol{\lambda}, \rho, \beta$ , threshold  $\varepsilon_1, \varepsilon_2$  and iteration index  $t = 1$  for outer loop
  - 2: **repeat:** outer loop
  - 3:   Initialize iteration index  $s = 1$  for inner loop.
  - 4:   **repeat:** inner loop
  - 5:     Update  $\mathbf{p}$  according to (37).
  - 6:     Update  $\mathbf{z}$  according to (40).
  - 7:     Update  $\boldsymbol{\lambda}$  according to (41).
  - 8:      $s = s + 1$ .
  - 9:   **until**  $\|\mathbf{p}[s] - \mathbf{p}[s-1]\|_2^2 \leq \varepsilon_1, \|\mathbf{z}[s] - \mathbf{z}[s-1]\|_2^2 \leq \varepsilon_1, \|\mathbf{p}[s] - \mathbf{z}[s]\|_2^2 \leq \varepsilon_1$ .
  - 10:    $t = t + 1$ .
  - 11:   Update  $\alpha$  according to (34).
  - 12: **until**  $\alpha[t] - \alpha[t-1] \leq \varepsilon_2$ .
- 

where the value of  $\mu_0$  is determined according to (33b). The details of solving this subproblem is shown in Appendix B.

#### 3) Subproblem with respect to $\boldsymbol{\lambda}$

The optimization for  $\boldsymbol{\lambda}$  is based on the multiplier update rule, i.e.,

$$\boldsymbol{\lambda}[s+1] = \boldsymbol{\lambda}[s] + \rho (\mathbf{p}[s+1] - \mathbf{z}[s+1]). \quad (41)$$

### C. Two-Stage Algorithm

So far, we have solved all subproblems with closed-form solutions and the proposed ADMM-based algorithm for (P2.1) is summarized in **Algorithm 1**.

In the first stage, we assume  $\mathbf{a}^H(\Omega_{\text{B2I}, k_1}, N_T) \mathbf{w}_{k_2} = 0, k_1 \neq k_2$  to satisfy (23b), which means orthogonality is achieved only by transmitting beamforming. In fact, we find reflective elements in some IRSs may not be assigned power after solving (P2.1), i.e.,  $\exists \tilde{k}, e_{\tilde{k}}^2 = 0$ . These activated reflective elements do not benefit the system performance but increase the difficulty of achieving channel orthogonality.

Therefore, in the second stage, we can relax the channel orthogonality constraint by not activating reflective elements on some IRSs. Specifically, after solving (P2.1), we divide  $\mathcal{K}$  into  $\tilde{\mathcal{K}} = \{\tilde{k} | e_{\tilde{k}}^2 = 0, \tilde{k} \in \mathcal{K}\}$  and  $\bar{\mathcal{K}} = \{\bar{k} | e_{\bar{k}}^2 > 0, \bar{k} \in \mathcal{K}\}$ ,  $\tilde{\mathcal{K}} + \bar{\mathcal{K}} = \mathcal{K}$ . Then, we set  $\boldsymbol{\Theta}_{\tilde{k}} = \mathbf{0}_{N \times N}, \mathbf{w}_{\tilde{k}} = \mathbf{0}_{N_T \times 1}, \forall \tilde{k} \in \tilde{\mathcal{K}}$  and resolve (P2.1) according to **Algorithm 1** while reducing the number of variables to be optimized (change subscript set from  $\forall k \in \mathcal{K}$  to  $\forall \bar{k} \in \bar{\mathcal{K}}$ ). We repeat the above process until one time after solving (P2.1), all activated reflective elements are assigned power.

**Algorithm 1** is computationally efficient because all variables are updated via closed-form expressions. Specifically, the complexity of updating  $\mathbf{p}, \mathbf{z}$  and  $\boldsymbol{\lambda}$  is  $\mathcal{O}(K^3), \mathcal{O}(I_{in}K)$  and  $\mathcal{O}(K)$ , respectively where  $I_{in}$  is the number of inner iterations required for convergence. Therefore, the overall complexity of **Algorithm 1** is  $\mathcal{O}(I_{out}(K^3 + I_{in}K))$  where  $I_{out}$  is the number of outer iterations required for convergence.

## V. MULTI-TARGET SYSTEM

In this section, we study the general multi-target localization scenario where multiple targets are located at arbitrary

locations and BS and IRSs utilize space beamforming to locate multiple targets in the same time-frequency dimension. For this general scenario, we propose an algorithm based on alternating optimization to solve the (P1).

### A. Dual Problem

By introducing an auxiliary  $\gamma$  variable to characterize the worst-case CRB among multi-target, (P1) can be equivalently rewritten as

$$(P3.1): \min_{\theta, \mathbf{W}} \frac{1}{\gamma} \quad (42a)$$

$$\text{s.t. CRB}(x_{T,q}, y_{T,q}) \leq \frac{1}{\gamma}, \forall q, \quad (42b)$$

$$(22b), (22c), (22d), (22e).$$

The QoS problem and max-min fairness (MMF) problem in communication are a pair of dual problems [28]. Similarly, we apply the above conclusions to the design of multi-target localization systems and formulate the following problem.

$$(P3.2): \min_{\theta, \mathbf{W}} \text{tr}(\mathbf{W}\mathbf{W}^H) \quad (43a)$$

$$\text{s.t. CRB}(x_{T,q}, y_{T,q}) \leq \frac{1}{\varphi}, \forall q, \quad (43b)$$

$$(22b), (22d), (22e).$$

The duality between (P3.1) and (P3.2) can be described as

$$P3.1 (P_{\max} = P_0) = \frac{1}{\gamma_0}, P3.2 \left( \frac{1}{\varphi} = \frac{1}{\gamma_0} \right) = P_0. \quad (44)$$

This duality implies that if we can obtain the solution for (P3.2), we can find the solution for (P3.1) by iteratively solving (P3.2) using a bisection search method until the transmit power equals  $P_{\max}$ . Moreover,  $\theta$  and  $\mathbf{W}$  are coupled in (22b) and (43b). Therefore, we utilize the two-stage algorithm to simplify (P3.2) similar to the single-target system and alternating optimization to solve it.

### B. Transmitting Beamforming Design

To satisfy orthogonality constraint  $\mathbf{a}^H(\Omega_{B2I,k_1}, N_T) \mathbf{w}_{k_2} = 0, k_1 \neq k_2$ , we still adopt the form of feasible solutions given in (29). Therefore,  $\|\mathbf{H}_{q,k,l} \mathbf{w}_k\|_2^2$  can be represented as  $\alpha_{I2I,q,k,l}^2 \alpha_{B2I,k}^2 e_k^2 M \|\mathbf{a}_{I2T,k,q}^H \Theta_k \mathbf{a}_{I2B,k}\|_2^2$ .

Let  $\alpha_{q,k,l} = \alpha_{I2I,q,k,l}^2 \alpha_{B2I,k}^2 M$ ,  $a_{q,k} = \sum_{l=1}^K a_{q,k,l}^2 \alpha_{q,k,l}$ ,  $b_{q,k} = \sum_{l=1}^K b_{q,k,l}^2 \alpha_{q,k,l}$  and  $c_{q,k} = \sum_{l=1}^K a_{q,k,l} b_{q,k,l} \alpha_{q,k,l}$ . By applying the change of variables  $\|\mathbf{a}_{I2T,k,q}^H \Theta_k \mathbf{a}_{I2B,k}\|_2^2 = \|\theta_k^T \text{diag}(\mathbf{a}_{I2T,k,q}^H) \mathbf{a}_{I2B,k}\|_2^2 \triangleq x_{q,k}$ , problem (P3.2) is reduced to

$$(P3.3): \min_{\mathbf{p}} \mathbf{h}^T \mathbf{p} \quad (45a)$$

$$\text{s.t. } \varphi(\mathbf{a}_q^T \mathbf{p} + \mathbf{b}_q^T \mathbf{p}) - \mathbf{a}_q^T \mathbf{p} \mathbf{b}_q^T \mathbf{p} + \mathbf{c}_q^T \mathbf{p} \mathbf{c}_q^T \mathbf{p} \leq 0, \forall q, \quad (45b)$$

$$p_k \geq 0, \forall k, \quad (45c)$$

where  $\mathbf{p} = [e_1^2, \dots, e_K^2]^T$ ,  $p_k$  denotes the  $k$ -th element in  $\mathbf{p}$ ,  $\mathbf{a}_q = [a_{q,1} x_{q,1}, \dots, a_{q,K} x_{q,k}]^T$ ,  $\mathbf{b}_q = [b_{q,1} x_{q,1}, \dots, b_{q,K} x_{q,k}]^T$  and  $\mathbf{c}_q = [c_{q,1} x_{q,1}, \dots, c_{q,k} x_{q,k}]^T$ . Note that (P3.3) is an indefinite quadratic optimization problem because of constrain (45b). Therefore, we adopt successive convex approximation (SCA) technique to approximate the indefinite quadratic term in constrain (45b). Specifically, in the  $r$ -th iteration, for a given feasible point  $\mathbf{p}^{(r)}$ , we have

$$\begin{aligned} \mathbf{a}_q^T \mathbf{p} \mathbf{b}_q^T \mathbf{p} - \mathbf{c}_q^T \mathbf{p} \mathbf{c}_q^T \mathbf{p} &= \mathbf{p}^T (\mathbf{A}_q - \beta_q \mathbf{I}) \mathbf{p} + \beta_q \mathbf{p}^T \mathbf{p} \\ &\geq \mathbf{p}^T (\mathbf{A}_q - \beta_q \mathbf{I}) \mathbf{p} + \beta_q \mathbf{p}^{(r)T} \mathbf{p}^{(r)} + 2\beta_q \mathbf{p}^{(r)T} (\mathbf{p} - \mathbf{p}^{(r)}), \end{aligned} \quad (46)$$

where  $\mathbf{A}_q = \frac{1}{2}(\mathbf{a}_q \mathbf{b}_q^T + \mathbf{b}_q \mathbf{a}_q^T)$  and  $\beta_q$  is the maximum eigenvalue of  $\mathbf{A}_q$ . By replacing the corresponding terms in the constrains (45b), (P3.3) can be transformed to a convex problem and solved by convex optimization tool such as CVX.

### C. Reflective Beamforming Design

For given transmitting beamforming  $\mathbf{W}$ , problem (P3.2) is reduced to a feasibility-check problem as follows.

$$(P3.4): \text{Find } \theta_k \quad (47a)$$

$$\begin{aligned} \text{s.t. } \varphi \left( \sum_{k=1}^K a_{q,k} p_k x_{q,k} + \sum_{k=1}^K b_{q,k} p_k x_{q,k} \right) \\ - \sum_{k=1}^K a_{q,k} p_k x_{q,k} \sum_{k=1}^K b_{q,k} p_k x_{q,k} \\ + \sum_{k=1}^K c_{q,k} p_k x_{q,k} \sum_{k=1}^K c_{q,k} p_k x_{q,k} \leq 0, \forall q, \end{aligned} \quad (47b)$$

(22d), (22e),

where  $x_{q,k} = \|\theta_k \text{diag}(\mathbf{a}_{I2T,k,q}^H) \mathbf{a}_{I2B,k}\|_2^2$ . Note that  $\theta_k$  appears in quartic form in (47b) and has non-convex unit-modulus constraints. Therefore, we apply SDR and SCA technique to relax (47b) and solve (P3.4) with a high-quality approximate solution. Specifically, by defining  $\mathbf{R}_k = \theta_k \theta_k^H$  and  $\mathbf{V}_{q,k} = \text{diag}(\mathbf{a}_{I2T,k,q}^H) \mathbf{a}_{I2B,k} \mathbf{a}_{I2B,k}^H \text{diag}(\mathbf{a}_{I2T,k,q})$ ,  $x_{q,k}$  is equivalent to  $\text{tr}(\mathbf{R}_k \mathbf{V}_{q,k})$  with constrains  $\mathbf{R}_k \succeq 0, \text{rank}(\mathbf{R}_k) = 1$ . Based on the above equivalent transformation, we have

$$x_{q,k} x_{q,k'} = \text{tr}(\mathbf{R}_k \mathbf{V}_{q,k}) \text{tr}(\mathbf{R}_{k'} \mathbf{V}_{q,k'}), \forall k, k' \in \mathcal{K}, \quad (48)$$

which is a non-convex function because of its bilinear form with respect to  $\mathbf{R}_k$  and  $\mathbf{R}_{k'}$ . Therefore, we replace  $\text{tr}(\mathbf{R}_k \mathbf{V}_{q,k}) \text{tr}(\mathbf{R}_{k'} \mathbf{V}_{q,k'})$  equivalently by  $f(\mathbf{R}_k, \mathbf{R}_{k'}) - g(\mathbf{R}_k, \mathbf{R}_{k'})$  with

$$f(\mathbf{R}_k, \mathbf{R}_{k'}) = (\text{tr}(\mathbf{R}_k \mathbf{V}_{q,k}) + \text{tr}(\mathbf{R}_{k'} \mathbf{V}_{q,k'}))^2 / 4, \quad (49)$$

$$g(\mathbf{R}_k, \mathbf{R}_{k'}) = (\text{tr}(\mathbf{R}_k \mathbf{V}_{q,k}) - \text{tr}(\mathbf{R}_{k'} \mathbf{V}_{q,k'}))^2 / 4. \quad (50)$$

Next, we apply SCA to linearize  $f(\mathbf{R}_k, \mathbf{R}_{k'})$  and  $g(\mathbf{R}_k, \mathbf{R}_{k'})$ , which can relax (47b) to a convex constraint. Specifically, in the  $r$ -th iteration, for a given feasible point  $(\mathbf{R}_k^{(r)}, \mathbf{R}_{k'}^{(r)})$ , the lower bounds of  $f(\mathbf{R}_k, \mathbf{R}_{k'})$  and

$$f(\mathbf{R}_k, \mathbf{R}_{k'}) \geq f(\mathbf{R}_k^{(r)}, \mathbf{R}_{k'}^{(r)}) + 2\text{tr}(\mathbf{R}_k^{(r)}\mathbf{V}_{q,k} + \mathbf{R}_{k'}^{(r)}\mathbf{V}_{q,k'}) \text{tr}(\mathbf{V}_{q,k}(\mathbf{R}_k - \mathbf{R}_k^{(r)}) + \mathbf{V}_{q,k'}(\mathbf{R}_{k'} - \mathbf{R}_{k'}^{(r)})) \triangleq f_{lb}(\mathbf{R}_k, \mathbf{R}_{k'}), \quad (51)$$

$$g(\mathbf{R}_k, \mathbf{R}_{k'}) \geq g(\mathbf{R}_k^{(r)}, \mathbf{R}_{k'}^{(r)}) + 2\text{tr}(\mathbf{R}_k^{(r)}\mathbf{V}_{q,k} - \mathbf{R}_{k'}^{(r)}\mathbf{V}_{q,k'}) \text{tr}(\mathbf{V}_{q,k}(\mathbf{R}_k - \mathbf{R}_k^{(r)}) - \mathbf{V}_{q,k'}(\mathbf{R}_{k'} - \mathbf{R}_{k'}^{(r)})) \triangleq g_{lb}(\mathbf{R}_k, \mathbf{R}_{k'}). \quad (52)$$

$g(\mathbf{R}_k, \mathbf{R}_{k'})$  are given in (51) and (52) by first-order Taylor expansion, respectively. Based on above relaxation, the bilinear form in (47b) can be approximated as

$$x_{q,k}x_{q,k'} \leq f(\mathbf{R}_k, \mathbf{R}_{k'}) - g_{lb}(\mathbf{R}_k, \mathbf{R}_{k'}), \quad (53)$$

$$-x_{q,k}x_{q,k'} \leq -f_{lb}(\mathbf{R}_k, \mathbf{R}_{k'}) + g(\mathbf{R}_k, \mathbf{R}_{k'}). \quad (54)$$

By replacing the corresponding terms  $x_{q,k}x_{q,k'}$  and  $-x_{q,k}x_{q,k'}$  in (47b) according to (53) and (54), respectively, and ignoring the rank-one constrain, (P3.4) can be reduced to

$$(P3.5): \text{Find } \mathbf{R}_k \quad (55a)$$

$$\begin{aligned} \text{s.t. } \varphi \left( \sum_{k=1}^K a_{q,k} p_k \text{tr}(\mathbf{R}_k \mathbf{V}_{q,k}) + \sum_{k=1}^K b_{q,k} p_k \text{tr}(\mathbf{R}_k \mathbf{V}_{q,k}) \right) \\ + \sum_{k=1}^K \sum_{k'=1}^K a_{q,k'} b_{q,k} p_k p_{k'} [g(\mathbf{R}_k, \mathbf{R}_{k'}) - f_{lb}(\mathbf{R}_k, \mathbf{R}_{k'})] \\ + \sum_{k=1}^K \sum_{k'=1}^K p_k p_{k'} f_{\text{sgn}}(c_{q,k}, c_{q,k'}, \mathbf{R}_k, \mathbf{R}_{k'}) \leq 0, \forall q, \end{aligned} \quad (55b)$$

$$[\mathbf{R}_k]_{n,n} = 1, \forall k, \forall n, \quad (55c)$$

$$\mathbf{R}_k \succeq 0, \forall k, \quad (55d)$$

where  $f_{\text{sgn}}(c_{q,k}, c_{q,k'}, \mathbf{R}_k, \mathbf{R}_{k'})$  is defined as

$$\begin{aligned} f_{\text{sgn}}(c_{q,k}, c_{q,k'}, \mathbf{R}_k, \mathbf{R}_{k'}) = \\ \begin{cases} c_{q,k}, c_{q,k'} [f(\mathbf{R}_k, \mathbf{R}_{k'}) - g_{lb}(\mathbf{R}_k, \mathbf{R}_{k'})], c_{q,k} c_{q,k'} \geq 0, \\ c_{q,k}, c_{q,k'} [f_{lb}(\mathbf{R}_k, \mathbf{R}_{k'}) - g(\mathbf{R}_k, \mathbf{R}_{k'})], c_{q,k} c_{q,k'} < 0. \end{cases} \end{aligned} \quad (56)$$

(P3.5) is a standard semi-definite programming problem and can be solved by a convex optimization tool such as CVX. Because we ignore the rank-one constrain and may obtain optimal solutions  $\mathbf{R}_k^*$  with  $\text{rank}(\mathbf{R}_k^*) > 1$ , Gaussian randomization can be used to achieve near-optimal performance.

To achieve better convergence, we introduce ‘‘residual variable’’  $r_q$  to characterize the difference between CRB  $(x_{T,q}, y_{T,q})$  and  $\frac{1}{\varphi}$  and transform the optimization objectives into an explicit function with respect to  $r_q$ . The modified

---

### Algorithm 2 Proposed Alternating Optimization Algorithm.

---

- 1: **Input:** Initialize  $\varphi_{\min}, \varphi_{\max}, \varphi = \sqrt{\varphi_{\max}\varphi_{\min}}$ , threshold  $\varepsilon_1, \varepsilon_2$  and iteration index  $t = 1$  for outer loop
  - 2: **repeat:** outer loop
  - 3:   Initialize iteration index  $s = 1$  for inner loop.
  - 4:   **repeat:** inner loop
  - 5:     Update  $\mathbf{p}$  by solving (P3.3).
  - 6:     Update  $\mathbf{R}_k$  by solving (P3.6).
  - 7:      $s = s + 1$ .
  - 8:     **until**  $\frac{\text{tr}(\mathbf{W}^{[t,s-1]}\mathbf{W}^{[t,s-1]H} - \mathbf{W}^{[t,s]}\mathbf{W}^{[t,s]H})}{\text{tr}(\mathbf{W}^{[t,s]}\mathbf{W}^{[t,s]H})} \leq \varepsilon_1$ .
  - 9:      $t = t + 1$ .
  - 10:    **if**  $\text{tr}(\mathbf{W}^{[t,s]}\mathbf{W}^{[t,s]H}) \leq P_{\max}$  **then**
  - 11:      $\varphi_{\max} = \varphi$ .
  - 12:    **else**
  - 13:      $\varphi_{\min} = \varphi$ .
  - 14:    **end if**
  - 15:     $\varphi = \sqrt{\varphi_{\max}\varphi_{\min}}$ .
  - 16: **until**  $\frac{|\text{tr}(\mathbf{W}^{[t,s]}\mathbf{W}^{[t,s]H}) - P_{\max}|}{P_{\max}} \leq \varepsilon_2$ .
- 

problem can be expressed as

$$(P3.6): \max_{\mathbf{R}_k, \{r_q\}} \sum_{q=1}^Q r_q \quad (57a)$$

$$\begin{aligned} \text{s.t. } \varphi \left( \sum_{k=1}^K a_{q,k} p_k \text{tr}(\mathbf{R}_k \mathbf{V}_{q,k}) + \sum_{k=1}^K b_{q,k} p_k \text{tr}(\mathbf{R}_k \mathbf{V}_{q,k}) \right) \\ + \sum_{k=1}^K \sum_{k'=1}^K a_{q,k'} b_{q,k} p_k p_{k'} [g(\mathbf{R}_k, \mathbf{R}_{k'}) - f_{lb}(\mathbf{R}_k, \mathbf{R}_{k'})] \\ + \sum_{k=1}^K \sum_{k'=1}^K p_k p_{k'} f_{\text{sgn}}(c_{q,k}, c_{q,k'}, \mathbf{R}_k, \mathbf{R}_{k'}) + r_q \leq 0, \forall q, \end{aligned} \quad (57b)$$

$$(55b), (55c).$$

(P3.5) and (P3.6) have the same feasible solution while Solving (P3.6) can make the alternating optimization algorithm converge faster.

#### D. Two-Stage Algorithm

So far, we have solved two subproblems in alternating optimization and the proposed alternating algorithm for problem (P1) is summarized in **Algorithm 2**, where  $\mathbf{W}^{[t,s]}$  is the output of  $\mathbf{W}$  in the  $t$ -th outer loop and the  $s$ -th loop of **Algorithm 2**.

Like the single-target system, we apply a two-stage algorithm framework to the multi-target system and the specific process is similar to section IV-C and omit it here.

TABLE I  
SIMULATION PARAMETERS

Parameter	Value	Parameter	Value	Parameter	Value
$N_t$	12	$N$	10	$M$	10
$K$	6	H <sub>BS</sub> /H <sub>IRS</sub>	50 m/30 m	$\kappa$	7 dBsm
$P_{\max}$	20 dBW	$\sigma_t^2$	-110 dBm	$\lambda$	0.3m

For **Algorithm 2**, the complexity is mainly dominated by solving the quadratic constrained quadratic programming and semidefinite programming problem. Specifically, the complexity of solving (P3.3) and (P3.6) is  $\mathcal{O}(I_{in1}K(K+1)^2)$  and  $\mathcal{O}(I_{in2}(KN^2Q + K^2N^4Q^2))$ , respectively where  $I_{in1}$  and  $I_{in2}$  are the number of inner iterations required for convergence. Therefore, the overall complexity of **Algorithm 2** is  $\mathcal{O}(I_{out}(I_{in1}K(K+1)^2 + I_{in2}(KN^2Q + K^2N^4Q^2)))$  is the number of outer iterations required for convergence where  $I_{out}$  is the number of inner iterations required for convergence.

## VI. SIMULATION RESULTS

In this section, we verify the effectiveness of our proposed algorithm multi-IRS collaborative localization system through numerical results. We consider a three-dimensional coordinate system in this section. The BS is located at (0, 0, 50m) while  $K$  IRSs and  $Q$  targets are located randomly distributed in the rectangular area whose coordinate is  $(-100 \leq x \leq 100, -100 \leq y \leq 100)$ . Other main system parameters are listed in Table I. We compare the proposed two-stage algorithm with the other three benchmarks:

- **One-stage:** All reflective elements on multiple IRSs are activated and **Algorithm 1** is applied only once.
- **Equal power allocation:** Power allocation is not designed and all IRSs receive equal energy with optimal phases.
- **Random phase shift:** The phase shift design of all reflective elements on the multiple IRSs is randomized with optimal power allocation.

### A. Single-Target System

1) *CRB Versus Number of IRSs:* In Fig. 3, we compare the CRB for location estimation of the single target versus the number of IRSs,  $K$ . First, it is observed that the CRB of both one-stage and equal power allocations schemes fluctuate as the number of IRSs increases. This is because more spatially distributed IRSs provide more spatial degrees of freedom to localization and signal propagation paths with less path loss. Moreover, there are more sensors on semi-passive IRSs, which provide a larger sample of observations from different angles. The above two reasons explain the positive impact of the increased number of IRSs on localization performance. On the other hand, we did not consider the design of multiple IRS deployments. Therefore, more IRSs will make it difficult to maintain orthogonality among different channels between IRSs and BS for active beamforming at BS. This leads to a reduction in the energy received by the IRSs and thus negatively affects the localization performance. Through the two-stage algorithm, reflective elements on some IRSs will

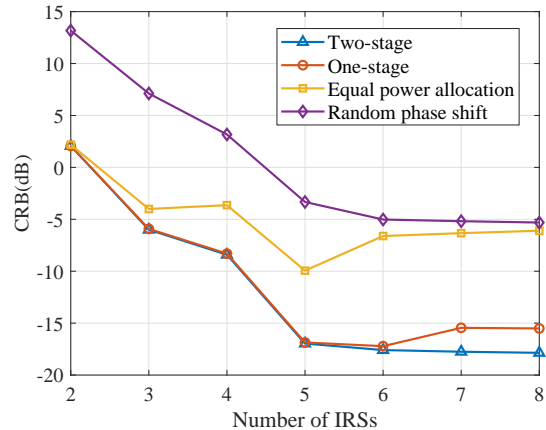


Fig. 3. CRB versus the number of IRSs.

not be activated. This avoids the drawbacks of multiple IRS and causes CRB to monotonically increase as the number of IRS increases.

Second, it is observed from Fig. 3 that when the number of IRSs increases to a certain value, the improvement in localization performance is no longer significant such as when the number of IRSs is raised to 5. This is because the first 5 IRSs already provide a good spatial angle for localizing that target, and only the sensors are functioning in the subsequent added IRSs. Finally, Fig. 3 demonstrates that the one-stage and two-stage algorithms perform comparably when the number of IRSs is small. This is because when the number of antennas is much larger than the number of IRSs, it is simple to achieve channel orthogonality through active beamforming. We will verify it from the case of increasing number of transmitting antennas in the next simulation.

2) *CRB Versus Number of Transmitting Antennas:* In Fig. 4, we compare the CRB for location estimation of the single target versus the number of transmitting antennas,  $N_t$  when  $K = 6$ . From Fig. 4, it is observed that the CRB of all schemes decreases monotonically as  $N_t$  increases. When  $N_t$  is slightly larger than the number of  $K$ , increasing  $N_t$  improves the performance of the one-stage and equal power allocation schemes significantly while The two-stage scheme achieves the best performance regardless of the number of transmitting antennas. This is because the two-stage scheme can avoid sensing signal interference from redundant IRSs. The design of the IRS reflection coefficients and the active beamforming both can bring about a gain of about 15 dB in system performance. Compared to the one-stage scheme, the advantage of the two-stage scheme is obvious when the values of  $N_t$  and  $K$  are close.

3) *CRB Versus Number of Elements or Sensors:* In Fig. 5, we compare the CRB for location estimation of the single target versus the number of reflective elements,  $N$  or sensors,  $M$ . To make it easier to observe the effect of both  $N$  and  $M$  on system performance, we set one of them to 10 and change the other from 10 to 70. it is observed that the CRB of all schemes decreases monotonically as  $N$  or  $M$  increases. However, the order of scaling down of CRB is different with respect to  $N$

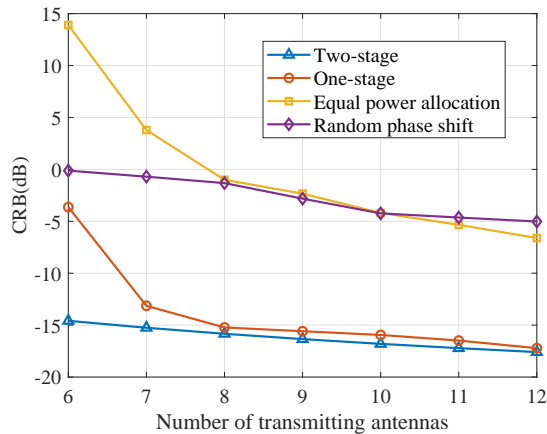


Fig. 4. CRB versus the number of transmitting antennas.

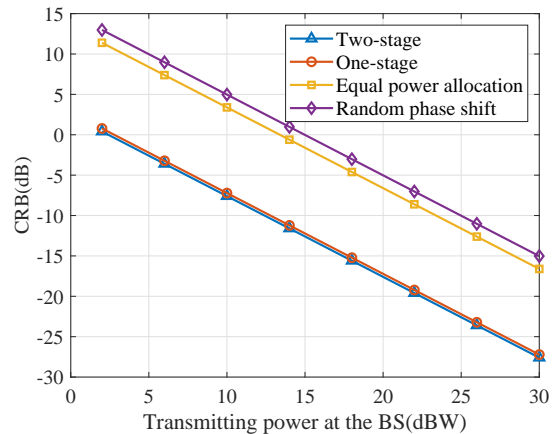


Fig. 6. CRB versus the maximum transmitting power.

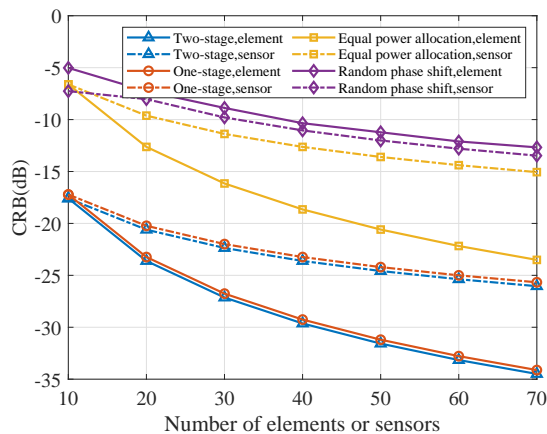


Fig. 5. CRB versus the number of elements or sensors.

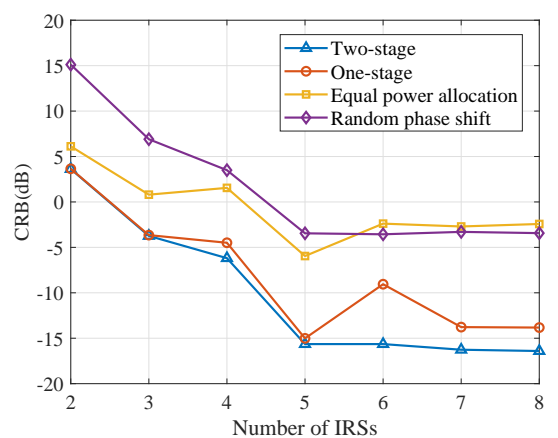


Fig. 7. CRB versus the number of IRSs in multi-target system.

and  $M$ . Specifically, CRB scales down with  $N$  and  $M$  approximately in the order of  $1/N^2$  and  $1/M$  except the random phase shift scheme, respectively. This is because reflective elements and sensors can achieve beamforming gain of  $\mathcal{O}(N^2)$  and  $\mathcal{O}(M)$ , respectively. However, for random phase shift scheme, reflective elements only achieve beamforming gain of  $\mathcal{O}(N)$ , which explains that the solid and dashed purple lines almost coincide with each other in Fig. 5.

4) *CRB Versus Maximum Transmitting Power*: In Fig. 6, we explored the relationship between CRB and maximum transmitting power,  $P_{\max}$ . It is observed that the CRB of all schemes decreases linearly and monotonically with increasing  $P_{\max}$ . This is because that Expression for CRB in (21) is inversely proportional to  $P_{\max}$ . All schemes are stable and insensitive to changes in  $P_{\max}$  and the difference between four schemes is constant regardless of  $P_{\max}$ .

### B. Multi-Target System

In this subsection, we consider a multi-target system and provide numerical simulation results to verify the effectiveness of the proposed algorithm with the other three schemes.

1) *CRB Versus Number of IRSs*: Fig. 7 shows the maximum CRB among multi-target versus the number of IRSs with

$Q = 8$ . Like the single-target scenario, the proposed two-stage algorithm alternating-based optimization achieves the best performance compared to the other three schemes and can monotonically increase the CRB as the number of IRSs increases. Compared to the single-target scenario, the performance gap between the proposed algorithm and the random phase design scheme becomes smaller. This is because the random phase design scheme will cause the beam formed by the IRSs to become directionless, and the energy of the sensing signal will be evenly distributed in space. When there are more targets to be located in space, the directionality of the optimal passive beamforming at IRSs will decrease.

2) *CRB Versus the Number of Targets*: Fig. 8 shows the maximum CRB among multi-target versus the number of targets. It can be observed that the proposed two-stage algorithm achieves the lowest CRB compared to other benchmark schemes regardless of the number of targets. The CRB of a multi-target system may not increase when some new targets that need to be localized are added, such as the addition of 4-th and 7-th targets in Fig. 8. This is because we restrict the target to be separable at time and the echo signals from different targets are interference-free with each other. Therefore, when new targets are added to some areas with relatively strong

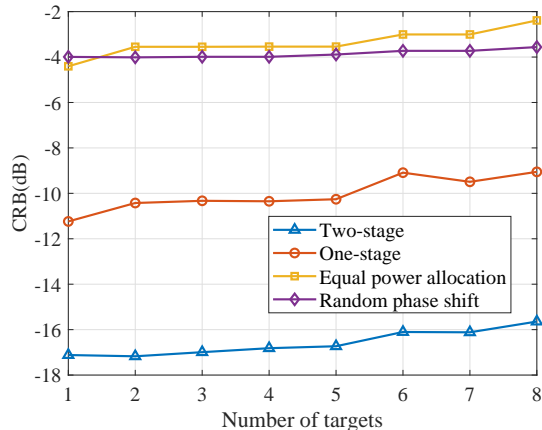


Fig. 8. CRB versus the number of targets in multi-target system.

energy coverage, the performance of the whole system will not be degraded, which is similar to the multicast communication system. In addition, we find that the performance of the random phase design scheme remains almost constant as the number of targets increases, which validates the previous conclusions.

## VII. CONCLUSIONS

In this paper, we investigate a novel TOA localization-based beamforming optimization problem for multiple IRSs collaborative localization system. Specifically, the active beamforming at the BS, passive beamforming at multiple IRSs, and IRS selection are jointly optimized in the framework of a two-stage algorithm to minimize the estimation CRB of the position of the target in Cartesian coordinates. For single- and multi-target scenarios, we propose ADMM-based and alternating optimization-based algorithms to achieve the best performance compared with other benchmark schemes, respectively. In addition, a number of conclusions that are useful in real system deployments and the gain in system performance with respect to the number of reflective elements and sensors, and the maximum transmitting power are revealed.

## APPENDIX A

### THE DERIVATION OF THE FIM IN (12)

The first derivative of  $p(\mathbf{r}_{\text{IRS}}|\boldsymbol{\tau})$  with respect to  $\tau_{q_1, k_1, l_1}$  is shown in (58), where we have applied the following properties to simplify.

$$\frac{\partial \mathbf{r}_{\text{IRS}, l}(t)}{\partial \tau_{q_1, k_1, l_1}} = 0, \quad \frac{\partial s(t - \tau_{q, k, l})}{\partial \tau_{q_1, k_1, l_1}} = 0, \quad \text{if } q \neq q_1 \text{ or } k \neq k_1. \quad (60)$$

Then, we apply the second derivative to (91) with respect to  $\tau_{q_2, k_2, l_2}$  and result is shown in (59), where we have applied the following properties to simplify.

$$\int_T \dot{s}_k(t - \tau_{q_1, k, l}) \dot{s}_k^H(t - \tau_{q_2, k, l}) = 0, \quad \text{if } q_1 \neq q_2, \quad (61)$$

$$\mathbb{E} \left\{ \mathbf{r}_{\text{IRS}, k}(t) - \sum_{q=1}^Q \sum_{k=1}^K \mathbf{H}_{q, k, l} \mathbf{w}_k s_k(t - \tau_{q, k, l}) \right\} = 0. \quad (62)$$

## APPENDIX B

### DETAILS OF ALGORITHM

The Lagrangian function of (P2.5) can be formulated as

$$L(\mathbf{z}, \mu_0, \boldsymbol{\mu}) = \frac{\rho}{2} \|\mathbf{p} - \mathbf{z}\|_2^2 - \beta \mathbf{z}^T \mathbf{z} + \boldsymbol{\lambda}^T (\mathbf{p} - \mathbf{z}) + \mu_0 (\mathbf{h}^T \mathbf{z} - P_{\max}) + \boldsymbol{\mu}^T \mathbf{z}, \quad (63)$$

where  $\mu_0$  and  $\boldsymbol{\mu}$  are Lagrange multipliers associated with constraint (33b) and (33c), respectively. According to KKT conditions, we have

$$\frac{\partial L}{\partial z_i} = (\rho - 2\beta) z_i - (\rho p_i + \lambda_i) + \mu_0 h_i + \mu_i = 0, \quad \forall i, \quad (64)$$

$$\mathbf{h}^T \mathbf{z} - P_{\max} = 0, \quad (65)$$

$$z_i \geq 0, \quad \forall i, \quad (66)$$

$$\mu_i \geq 0, \quad \forall i, \quad (67)$$

$$\mu_i z_i = 0, \quad \forall i. \quad (68)$$

Based on (64) and (67), we have

$$\mu_i = (\rho p_i + \lambda_i) - (\rho - 2\beta) z_i - \mu_0 h_i \geq 0, \quad \forall i. \quad (69)$$

According to complementary relaxation condition (68),

$$[(\rho p_i + \lambda_i) - (\rho - 2\beta) z_i - \mu_0 h_i] z_i = 0, \quad \forall i. \quad (70)$$

Then, we can discuss the solution based on the value of  $\mu_0$

**Case 1:**  $\mu_0 \geq \frac{\rho p_i + \lambda_i}{h_i}$

It is obvious that  $(\rho p_i + \lambda_i) - (\rho - 2\beta) z_i - \mu_0 h_i \geq 0$  because  $z_i \geq 0$  and  $\rho > 2\beta$ . Therefore, the sufficient and necessary conditions of (68) is  $z_i = 0$ .

**Case 2:**  $\mu_0 < \frac{\rho p_i + \lambda_i}{h_i}$

If  $z_i = 0$ , (68) must not hold. Therefore,

$$z_i = \frac{\rho p_i + \lambda_i - \mu_0 h_i}{\rho - 2\beta}, \quad (71)$$

which ensures (68) holds.

The final problem is to determine the value of  $\mu_0$ . Firstly, we are unable to determine the numerical relationship between  $\mu_0$  and  $\frac{\rho p_i + \lambda_i}{h_i}, \forall i$ . Therefore we assume that  $\mu_0 < \frac{\rho p_i + \lambda_i}{h_i}, \forall i$ . Recalling (65) and (71), we have

$$\mu_0 = \frac{-(\rho - 2\beta) P_{\max} + \sum_{i=1}^K (\rho p_i h_i + \lambda_i h_i)}{\sum_{i=1}^K h_i^2}. \quad (72)$$

Substituting (72) into (71), we can obtain  $z_i$ . If, according to the calculations,  $\exists i', z_{i'} \leq 0$ , we set  $z_{i'} = 0, \forall i'$  and update  $\mu_0$  and recalculate  $z_i$  until  $z_i \geq 0, \forall i$ .

## REFERENCES

- [1] A. Behravan, V. Yajnanarayana, M. F. Keskin, H. Chen, D. Shrestha, T. E. Abruđan, T. Svensson, K. Schindhelm, A. Wolfgang, S. Lindberg, and H. Wymeersch, "Positioning and sensing in 6G: Gaps, challenges, and opportunities," *IEEE Veh. Technol. Mag.*, vol. 18, no. 1, pp. 40–48, Dec. 2023.
- [2] I. Yaqoob, L. U. Khan, S. M. A. Kazmi, M. Imran, N. Guizani, and C. S. Hong, "Autonomous driving cars in smart cities: Recent advances, requirements, and challenges," *IEEE Network*, vol. 34, no. 1, pp. 174–181, Jan. 2020.
- [3] Y. Alghamdi, A. Munir, and H. M. La, "Architecture, classification, and applications of contemporary unmanned aerial vehicles," *IEEE Consumer Electronics Mag.*, vol. 10, no. 6, pp. 9–20, Nov. 2021.

$$\begin{aligned}
& \frac{\partial \log p(\mathbf{r}_{\text{IRS}}|\boldsymbol{\tau})}{\partial \tau_{q_1, k_1, l_1}} = \\
& = \frac{\frac{1}{\sigma_l^2} \sum_{l=1}^K \int_T \left[ \mathbf{r}_{\text{IRS}, l}(t) - \sum_{q=1}^Q \sum_{k=1}^K \mathbf{H}_{q, k, l} \mathbf{w}_k s_k(t - \tau_{q, k, l}) \right]^H \left[ \mathbf{r}_{\text{IRS}, l}(t) - \sum_{q=1}^Q \sum_{k=1}^K \mathbf{H}_{m, k, l} \mathbf{w}_k s_k(t - \tau_{q, k, l}) \right] dt}{\partial \tau_{q_1, k_1, l_1}} \\
& = \frac{1}{\sigma_l^2} \int_T \left\{ \left[ \mathbf{r}_{\text{IRS}, l}(t) - \sum_{q=1}^Q \sum_{k=1}^K \mathbf{H}_{q, k, l} \mathbf{w}_k s_k(t - \tau_{q, k, l}) \right]^H \frac{\partial [\mathbf{H}_{q_1, k_1, l_1} \mathbf{w}_{k_1} s_{k_1}(t - \tau_{q_1, k_1, l_1})]}{\partial \tau_{q_1, k_1, l_1}} \right. \\
& \left. + \frac{\partial [\mathbf{H}_{q_1, k_1, l_1} \mathbf{w}_{k_1} s_{k_1}(t - \tau_{q_1, k_1, l_1})]^H}{\partial \tau_{q_1, k_1, l_1}} \left[ \mathbf{r}_{\text{IRS}, l}(t) - \sum_{q=1}^Q \sum_{k=1}^K \mathbf{H}_{q, k, l} \mathbf{w}_k s_k(t - \tau_{q, k, l}) \right] \right\} dt,
\end{aligned} \tag{58}$$

$$\begin{aligned}
& \mathbb{E} \left\{ \frac{\partial^2 \log p(\mathbf{r}_{\text{IRS}}|\boldsymbol{\tau})}{\partial \tau_{q_1, k_1, l_1} \partial \tau_{q_2, k_2, l_2}} \right\} = \frac{1}{\sigma_n^2} \mathbb{E} \left\{ \int_T \frac{[\partial \mathbf{H}_{q_2, k_2, l_2} \mathbf{w}_{k_2} s_{k_2}(t - \tau_{q_2, k_2, l_2})]^H}{\partial \tau_{q_2, k_2, l_2}} \frac{\partial [\mathbf{H}_{q_1, k_1, l_1} \mathbf{w}_{k_1} s_{k_1}(t - \tau_{q_1, k_1, l_1})]}{\partial \tau_{q_1, k_1, l_1}} \right. \\
& \left. + \frac{[\partial \mathbf{H}_{q_1, k_1, l_1} \mathbf{w}_{k_1} s_{k_1}(t - \tau_{q_1, k_1, l_1})]^H}{\partial \tau_{q_1, k_1, l_1}} \frac{\partial [\mathbf{H}_{q_2, k_2, l_2} \mathbf{w}_{k_2} s_{k_2}(t - \tau_{q_2, k_2, l_2})]}{\partial \tau_{q_2, k_2, l_2}} dt \right\} \\
& = \begin{cases} 0, l_1 \neq l_2 \text{ or } q_1 \neq q_2, \\ \frac{1}{\sigma_l^2} \text{Re} \int_T \left[ \mathbf{H}_{q_1, l_1, k} \mathbf{H}_{q_2, l_2, k}^H \sum_{k=1}^K \mathbf{w}_k^H \dot{s}_k^H(t - \tau_{q_1, l_1, k}) \sum_{k=1}^K \mathbf{w}_k \dot{s}_k(t - \tau_{q_2, l_2, k}) \right] dt, \text{ others,} \end{cases}
\end{aligned} \tag{59}$$

- [4] H. K. Dureppagari, C. Saha, H. S. Dhillon, and R. M. Buehrer, "Ntn-based 6G localization: Vision, role of LEOs, and open problems," *IEEE Wireless Communications*, vol. 30, no. 6, pp. 44–51, Dec. 2023.
- [5] S. Vakalis, S. Mghabghab, and J. A. Nanzer, "Fourier domain millimeter-wave imaging using noncooperative 5G communications signals," *IEEE Trans. Antennas Propag.*, vol. 70, no. 10, pp. 8872–8882, May 2022.
- [6] W. Chen, L. Li, Z. Chen, T. Quek, and S. Li, "Enhancing THz/mmWave network beam alignment with integrated sensing and communication," *IEEE Commun. Lett.*, vol. 26, no. 7, pp. 1698–1702, Jul. 2022.
- [7] Q. Wu and R. Zhang, "Intelligent reflecting surface enhanced wireless network via joint active and passive beamforming," *IEEE Trans. Wireless Commun.*, vol. 18, no. 11, pp. 5394–5409, Aug. 2019.
- [8] Q. Wu and R. Zhang, "Towards smart and reconfigurable environment: Intelligent reflecting surface aided wireless network," *IEEE Commun. Mag.*, vol. 58, no. 1, pp. 106–112, Jan. 2020.
- [9] W. Lu, Q. Lin, N. Song, Q. Fang, X. Hua, and B. Deng, "Target detection in intelligent reflecting surface aided distributed mimo radar systems," *IEEE Sensors Lett.*, vol. 5, no. 3, pp. 1–4, Feb. 2021.
- [10] H. Zhang, H. Zhang, B. Di, K. Bian, Z. Han, and L. Song, "Metalocalization: Reconfigurable intelligent surface aided multi-user wireless indoor localization," *IEEE Trans. Wireless Commun.*, vol. 20, no. 12, pp. 7743–7757, Jun. 2021.
- [11] A. Taha, M. Alrabeiah, and A. Alkhateeb, "Enabling large intelligent surfaces with compressive sensing and deep learning," *IEEE Access*, vol. 9, pp. 44 304–44 321, Mar. 2021.
- [12] Y. Lin, S. Jin, M. Matthaiou, and X. You, "Tensor-based algebraic channel estimation for hybrid IRS-assisted MIMO-OFDM," *IEEE Trans. Wireless Commun.*, vol. 20, no. 6, pp. 3770–3784, Jan. 2021.
- [13] X. Shao, C. You, W. Ma, X. Chen, and R. Zhang, "Target sensing with intelligent reflecting surface: Architecture and performance," *IEEE J. Sel. Areas Commun.*, vol. 40, no. 7, pp. 2070–2084, Mar. 2022.
- [14] S. Buzzi, E. Grossi, M. Lops, and L. Venturino, "Radar target detection aided by reconfigurable intelligent surfaces," *IEEE Signal Processing Lett.*, vol. 28, pp. 1315–1319, Jun. 2021.
- [15] K. Meng, Q. Wu, R. Schober, and W. Chen, "Intelligent reflecting surface enabled multi-target sensing," *IEEE Trans. Commun.*, vol. 70, no. 12, pp. 8313–8330, Nov. 2022.
- [16] M. Hua, Q. Wu, W. Chen, Z. Fei, H. C. So, and C. Yuen, "Intelligent reflecting surface-assisted localization: Performance analysis and algorithm design," *IEEE Wireless Commun. Lett.*, vol. 13, no. 1, pp. 84–88, Jan. 2024.
- [17] Q. Peng, Q. Wu, W. Chen, S. Ma, M.-M. Zhao, and O. A. Dobre, "Semi-passive intelligent reflecting surface enabled sensing systems," *arXiv preprint arXiv:2402.03042*, 2024.
- [18] X. Song, J. Xu, F. Liu, T. X. Han, and Y. C. Eldar, "Intelligent reflecting surface enabled sensing: Cramér-rao bound optimization," *IEEE IEEE Trans. Signal Process.*, vol. 71, pp. 2011–2026, May. 2023.
- [19] C. Pan, H. Ren, K. Wang, J. F. Kolb, M. Elkhachan, M. Chen, M. Di Renzo, Y. Hao, J. Wang, A. L. Swindlehurst, X. You, and L. Hanzo, "Reconfigurable intelligent surfaces for 6G systems: Principles, applications, and research directions," *IEEE Commun. Mag.*, vol. 59, no. 6, pp. 14–20, Jun. 2021.
- [20] Z. Yang, M. Chen, W. Saad, W. Xu, M. Shikh-Bahaei, H. V. Poor, and S. Cui, "Energy-efficient wireless communications with distributed reconfigurable intelligent surfaces," *IEEE Trans. Wireless Commun.*, vol. 21, no. 1, pp. 665–679, Jul. 2022.
- [21] L. Yang, Y. Yang, D. B. d. Costa, and I. Trigui, "Outage probability and capacity scaling law of multiple RIS-aided networks," *IEEE Wireless Commun. Lett.*, vol. 10, no. 2, pp. 256–260, Sept. 2021.
- [22] T. V. Nguyen, D. N. Nguyen, M. D. Renzo, and R. Zhang, "Leveraging secondary reflections and mitigating interference in multi-IRS/RIS aided wireless networks," *IEEE Trans. Wireless Commun.*, vol. 22, no. 1, pp. 502–517, Jan. 2023.
- [23] W. Mei and R. Zhang, "Multi-beam multi-hop routing for intelligent reflecting surfaces aided massive MIMO," *IEEE Trans. Wireless Commun.*, vol. 21, no. 3, pp. 1897–1912, Sept. 2022.
- [24] S. Lyu, X. Hu, C. Liu, and M. Peng, "IRS-aided location sensing and beamforming in ISAC systems: Distributed or not?" *IEEE Trans. Veh. Technol.*, pp. 1–15, Apr. 2024.
- [25] Y. Fang, S. Zhang, X. Li, X. Yu, J. Xu, and S. Cui, "Multi-IRS-enabled integrated sensing and communications," *IEEE Trans. Commun.*, pp. 1–1, Apr. 2024.
- [26] H. Godrich, A. M. Haimovich, and R. S. Blum, "Target localization accuracy gain in MIMO radar-based systems," *IEEE Trans. Inf. Theory*, vol. 56, no. 6, pp. 2783–2803, May 2010.
- [27] W. Yi, T. Zhou, Y. Ai, and R. S. Blum, "Suboptimal low complexity joint multi-target detection and localization for non-coherent MIMO radar with widely separated antennas," *IEEE Trans. Signal Process.*, vol. 68, pp. 901–916, Jan. 2020.
- [28] E. Chen and M. Tao, "ADMM-based fast algorithm for multi-group multicast beamforming in large-scale wireless systems," *IEEE Trans. Commun.*, vol. 65, no. 6, pp. 2685–2698, Mar. 2017.

